IV International Conference on Computational Methods for Coupled Problems in Science and Engineering
COUPLED PROBLEMS 2011
M. Papadrakakis, E. Oñate and B. Schrefler (Eds)

NUMERICAL SIMULATIONS OF PARTICLES IN A SHEAR FLOW

NICOLAS VERDON*, PATRICE LAURE*, ALINE LEFEBVRE-LEPOT† AND LAURENT LOBRY‡

* Laboratoire J.-A. Dieudonné, CNRS UMR 6621, Université de Nice-Sophia Antipolis
Parc Valrose, 06108 Nice Cedex 02, France
Email: {nicolas.verdon,patrice.laure}@unice.fr

† Centre de Mathématiques Appliquées (CMAP), Ecole Polytechnique
Route de Saclay, 91128 Palaiseau, France
Email: aline.lefebvre@polytechnique.edu

‡ Laboratoire de Physique de la Matière Condensée (LPMC), Université de Nice-Sophia Antipolis
Parc Valrose, 06108 Nice Cedex 02, France
Email: laurent.lobry@unice.fr

Key words: Suspension, contact, viscous contact model, fluid-structure interaction, immersed domain method

Abstract. In this paper, we present an immersed domain approach coupled with a viscous contact model for studying the rheological behaviour of dense suspensions in a shear flow. We here demonstrate the importance of contact modelling as well as the choice of the boundary conditions on the macroscopic properties of the suspension.

1 INTRODUCTION

In the field of materials forming, as well as in many other industrial fields, determining the rheological behaviour of dense suspensions remains of great importance. Lots of different computational methods can be used to handle such fluid-structure interactions but in this work, we propose to study the behaviour of solid particles in a shear flow with the immersed domain method. First introduced in the late 90's by Glowinski *et al.* [1], this kind of methods encounters an increasing success in fluide-structure of multiphase problems because it allows to treat these problems with an Eulerian approach on the whole domain.
In order to be able to study accurately problems with a large amount of particles, we focused first our analysis to the description of the contact for a few particles in a shear flow. To avoid particle overlapping during displacement of particles, we implemented contact models such as an inelastic collisions model and the viscous contact model introduced by Maury [2] and intensively studied by Lefebvre [3] for granular applications.

We then focused our analysis on the choice of the boundary conditions for describing dense suspensions in a representative way. We present in details the way of extending the computational domain and we insist on the description of sliding biperiodic conditions of Lee-Edwards [4].
In the last part of this article, we present some representative results that confirm the different choices we have done in this study. First, the importance of the contact modelling will be pointed out with a 3D example of 13 particles in a shear flow. Finally, some examples of suspensions will also demonstrate the rheological modifications due to the choice of boundary conditions.

2 NUMERICAL MODEL

In this part, we briefly describe the main features of the numerical model that has been used for this study. The importance of the contact modelling is therefore explained at the end of the section.

2.1 The immersed domain approach

The immersed domain method is achieved by splitting the computational domain Ω into two subdomains Ω_f and Ω_s for respectively the fluid and solid parts (see Figure 1). In the case of multiple particles, the solid domain is the union of domains corresponding to each particle, namely $\Omega_s = \bigcup_i^N \Omega_{s_i}$ for N particles.

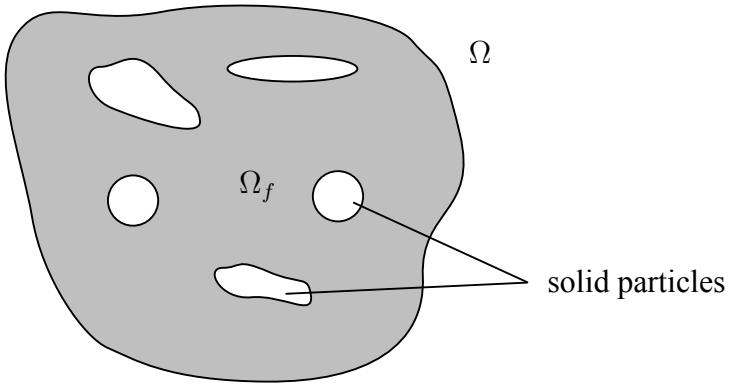

Figure 1: Schematic representation of computational domain

The interface Γ_s between the two phases is described by the zero isosurface of a distance function:

$$\alpha(\mathbf{x}, t) = \begin{cases} > 0 \text{ if } \mathbf{x} \in \Omega_s \\ < 0 \text{ if } \mathbf{x} \notin \Omega_s \end{cases} \tag{1}$$

which allows to define a "smooth" characteristic function:

$$\mathbb{I}(x,t) = \begin{cases} = 1 \text{ if } \alpha(x) > e \\ = \dfrac{\alpha}{e} \text{ if } 0 < \alpha(x) < e \\ = 0 \text{ if } \alpha < 0 \end{cases} \tag{2}$$

where e the mixing thickness depends on the mesh size around the interface. In addition, the viscosity η will be defined thanks to a mixing relation:

$$\eta = \mathbb{I}\eta_s + (\mathbb{E} - \mathbb{I})\eta_f \tag{3}$$

where η_f is the fluid viscosity and $\eta_s \simeq r\eta_f$ the solid viscosity (or penalisation factor) usually taken much bigger than η_f ($r \approx 10^3$).

2.2 Governing equations

Neglecting inertia and gravity, the fluid-solid problem can be written with the following set of equations:

$$\begin{cases} \nabla \,.\, \sigma & = & 0 \\ \nabla \,.\, \mathbf{u} & = & 0 \\ \sigma & = & 2\eta_f \, \dot{\epsilon}(\mathbf{u}) - p\mathbf{E} \\ [[\mathbf{u}]]_{\Gamma_s} & = & 0 \\ [[\sigma.\mathbf{n}]]_{\Gamma_s} & = & 0 \\ \mathbf{u} & = & \mathbf{u}_\Gamma \quad \text{on the external boundary } \Gamma \end{cases} \tag{4}$$

where $\mathbf{u}$ is the fluid velocity, $\dot{\epsilon}(\mathbf{v})$ the rate of strain tensor, σ the stress tensor, p the pressure, η_f the fluid viscosity (the symbol $[[f]]_{\Gamma_s}$ means the jump of scalar f across the interface Γ_s). Patankar *et al.* [5] have proposed to extend the above Stokes equation to the solid domain thanks to a Lagrange multiplier by using the rigidity condition $\dot{\epsilon}(\mathbf{v}) = 0$ on Ω_s. In this way, the motion in solid domain Ω_s corresponds to a fluid motion with an additional stress field. This is equivalent to take the stress tensor σ inside the solid domain of the form

$$\sigma = 2\eta_s \, \dot{\epsilon}(\mathbf{u}) - p\,\mathbb{E} + \dot{\epsilon}(\lambda) \tag{5}$$

2.3 Weak formulation of the FSI problem

The equation (5) allows us to write the foolowing weak formulation over the whole computational domain Ω, where Dirichlet boundary conditions are imposed:
Find $\left(\mathbf{u},\, p,\, \lambda\right)$ such that $\forall \left(\mathbf{v},\, q,\, \mu\right) \in \mathcal{H}^1(\Omega) \times \mathcal{L}^2_0(\Omega) \times \mathcal{H}^1(\Omega_s)$:

$$\begin{cases} 0 & = & \displaystyle\int_\Omega 2\eta \, \dot{\epsilon}(\mathbf{u}) : \dot{\epsilon}(\mathbf{v}) d\Omega \, - \, \int_\Omega p \nabla.\mathbf{v} d\Omega + \int_{\Omega_s} \dot{\epsilon}(\lambda) : \dot{\epsilon}(\mathbf{v}) d\Omega \\ 0 & = & \displaystyle\int_\Omega q \, \nabla.\mathbf{u} d\Omega \\ 0 & = & \displaystyle\int_{\Omega_s} \dot{\epsilon}(\mu) : \dot{\epsilon}(\mathbf{v}) d\Omega \end{cases} \tag{6}$$

This formulation corresponds to an augmented Lagrangian where λ is the Lagrange multiplier and η_s the penalisation factor. This is solved by an Uzawa algorithm [6].

2.4 Contact modelling

The particles displacement is then achieved by using the velocity of the fluid, solution of (6), and a lagrangian approach. Namely the displacement $\mathbf{X}_i$ of particle i at time $t^{n+1} = t^n + \Delta t$ is computed with the second order Adams-Bashfort scheme:

$$\mathbf{X}_i(t^{n+1}) = \mathbf{X}_i(t^n) + \frac{\Delta t}{2}\left[3\mathbf{u}(\mathbf{X}_i(t^n), t^n) - \mathbf{u}(\mathbf{X}_i(t^{n-1}), t^{n-1})\right] \tag{7}$$

It has been observed that overlapping can occur during this step, mathematically the distance D_{ij} between two particles i and j can become negative. In order to avoid this non-physical behaviour, we used the viscous contact model that has been introduced by Maury [2] and Lefebvre [3]. This model can be seen as a predictor–corrector model based on the action of the lubrication force. Indeed, the velocity field $\mathbf{u}^*$ obtained by solving Equation (6) does not take into account contacts. Hence, this *predicted velocity* will be corrected in a way that it satisfies the non-overlapping condition, namely by solving:

$$\frac{1}{2}\left|\mathbf{u}^n - \mathbf{u}^*\right|^2 = \min_{\mathbf{v}\in K(\mathbf{X}^n, \gamma_{ij}^n)} \frac{1}{2}\left|\mathbf{v} - \mathbf{u}^*\right|^2 \tag{8}$$

where K is the space of admissible velocity defined by

$$K(\mathbf{X}^n, \gamma_{ij}^n) = \left\{ \mathbf{v} \;\middle|\; \begin{array}{l} D_{ij}^n + \Delta t(\mathbf{v}_j - \mathbf{v}_i)\cdot \mathbf{e}_{ij}^n \geq 0 \text{ if } \gamma_{ij}^n = 0 \\ \\ D_{ij}^n + \Delta t(\mathbf{v}_j - \mathbf{v}_i)\cdot \mathbf{e}_{ij}^n \leq 0 \text{ if } \gamma_{ij}^n < 0 \end{array} \right\} \tag{9}$$

The contact between particles is then described by a new variable γ_{ij} which can be seen as a microscopic distance between particles i and j:

$$\gamma_{ij}^n \begin{cases} < 0 \text{ if there is contact between particles } i \text{ and } j \\ = 0 \text{ else} \end{cases} \tag{10}$$

Let us define the functional J as follows:

$$J(\mathbf{v}) = \frac{1}{2}\left|\mathbf{v} - \mathbf{u}^*\right|^2 = \frac{1}{2}\mathbf{M}\mathbf{v}\cdot\mathbf{v} - \mathbf{M}\mathbf{u}^*\cdot\mathbf{v} \tag{11}$$

where $\mathbf{M} = \mathrm{diag}(\ldots, m_i, \cdots, m_j, \cdots)$ is the mass matrix. Then the Lagrangian of $J(\mathbf{u})$ for two particles i and j has the following form:

$$\begin{aligned} \mathcal{L}(\mathbf{v}, \lambda_{ij}^{\pm}) \;&=\; J(\mathbf{v}) - \lambda_{ij}^{+}\left(D_{ij} + \Delta t(\mathbf{v}_j - \mathbf{v}_i)\cdot\mathbf{e}_{ij}\right) \\ &\quad -\; \lambda_{ij}^{-}\left(-D_{ij} - \Delta t(\mathbf{v}_j - \mathbf{v}_i)\cdot\mathbf{e}_{ij}\right) \end{aligned} \tag{12}$$

where λ_{ij}^+ and λ_{ij}^- are the Lagrange multipliers associated to the contact constraints. Finally, by solving $\dfrac{\partial \mathcal{L}}{\partial \mathbf{v}_i} = 0$ and $\dfrac{\partial \mathcal{L}}{\partial \mathbf{v}_j} = 0$, we obtain the two following relations:

$$\begin{cases} m_i \mathbf{u}_i^n = m_i \mathbf{u}_i^* - (\lambda_{ij}^+ - \lambda_{ij}^-)\Delta t \ \mathbf{e}_{ij} \\ m_j \mathbf{u}_j^n = m_j \mathbf{u}_j^* + (\lambda_{ij}^+ - \lambda_{ij}^-)\Delta t \ \mathbf{e}_{ij} \end{cases} \tag{13}$$

under the conditions :

$$\lambda_{ij}^{\pm}(D_{ij} + \Delta t(\mathbf{u}_j^n - \mathbf{u}_i^n) \cdot \mathbf{e}_{ij}) = 0 \ \text{ with } \ \lambda_{ij}^+ \geq 0 \ \text{ and } \ \lambda_{ij}^- \leq 0 \tag{14}$$

which is also solved with an Uzawa procedure.
Then the correction step of the viscous contact model involves the Fundamental Principal of the Dynamics where the lubrication forces are taken into account. The evolution of the contact parameter γ_{ij} can be obtain after some basic calculus, see [7] for more details:

$$\frac{d\gamma_{ij}}{dt} = -\frac{1}{a^2}\lambda_{ij} \quad \text{with} \quad \lambda_{ij} = \lambda_{ij}^+ - \lambda_{ij}^-. \tag{15}$$

Note that the inelastic collisions model can be obtained from these expressions by imposing $\gamma_{ij} = 0$, that is to say $\lambda_{ij} > 0$.

3 DESCRIPTION OF THE BOUNDARY CONDITIONS

When increasing the concentration of solid particles in a suspension, we notice that the choice of the boundary conditions becomes of great importance. Indeed, the number of contacts between particles is also increased and hence the boundary conditions (BC) can affect the rheology of the suspension. In this section, we present the different choices that can be made by focusing particularly on the Lee-Edwards' biperiodic conditions.

3.1 Representative elementary volume

In the numerical study of suspension, it is important to work on a suitable representative elementary volume (REV). Ideally, one would like to be able to know the behaviour of suspensions in an infinite domain, practically by working on a very large computational domain Ω_t with boundaries extremely far from the domain of interest Ω_{REV}, as depicted in figure 2. Unfortunately, this kind of approach is nowadays very computationaly expensive, especially for 3D simulations, that is why we have to deal with the boudary conditions in order to have a representative domain. For low concentrated suspension, it is common to work on a small domain but if the concentration increases, it is no more representative. Indeed, in Ω_{REV} the influence of the particles from the domain $\Omega_t \cap \overline{\Omega}_{REV}$ are taken into account whereas in a small domain of size Ω_{REV}, the particles inside the domains do not see particles from outside.

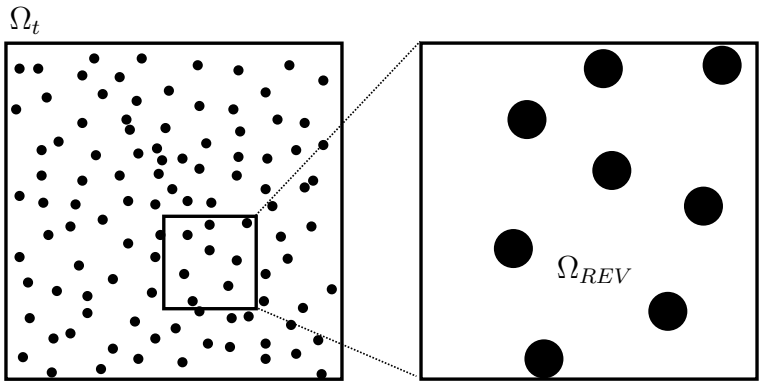

Figure 2: Ideal computational domain and Representative Elementary Volume

3.2 Extension of the computational domain

In this article, we focused our work on a shear flow in a cavity, as represented in figure 3. The velocities on the upper and lower boundaries are hence imposed in order to get the desired

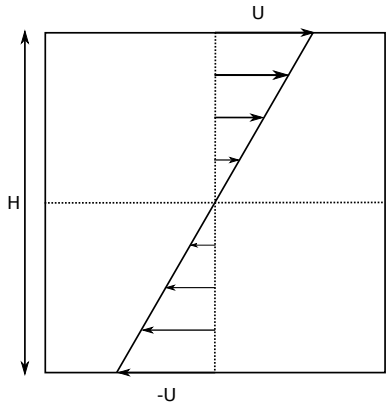

Figure 3: Configuration of the shear flow

shear rate whereas the vertical velocities in the lateral walls are equal to zero. As explained in the previous section, we mainly use small computational domains Ω_0 like 4(a) for dilute suspensions. In this case, we impose periodic conditions on the horizontal directions. That means that each particle that goes outside the domain through vertical walls re-enters in the domain from the other side. However, because of the zero vertical velocity imposed in these walls, the velocities can be badly estimated. Indeed, even if the motion of particles is periodic, the computed velocity is not periodic, that is why we proposed to extend the computational domain in the x–direction as depicted in figure 4(b). Thanks to this extension, the particles near a boundary see those from the opposite side.

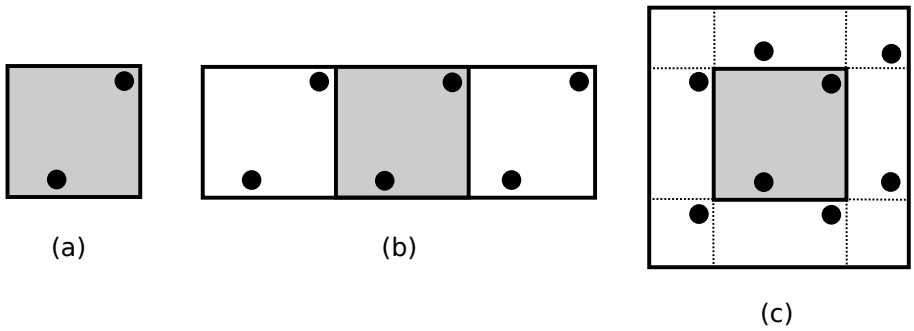

Figure 4: Extension of the computational domain : (a) original domain CL $(0,0)$, (b) domain extended in the x–direction CL $(1,0)$, (c) domain with sliding biperiodic boundary conditions CL $(1/2,1/2)$

In practice, we can extend the computational domain as much as we want and k_x and k_y are the two parameters which characterise the extension of the computational domain in respectively x and y– direction. For example, in the configuration 4(b), $k_x = 1$ and $k_y = 0$. The domain is extended in x–direction of length H in both sides of the original domain so that the new domain is then three times larger than the original domain Ω_0. The way of duplicating particles follows these rules:

$$\text{if } x_\alpha + H \in [H, H + k_{x_\alpha} H], \text{ then } \quad x_\alpha^+ = x_\alpha + H, \qquad \text{where } x_\alpha = x \text{ or } y \tag{16}$$

$$\text{if } x_\alpha - H \in [H - k_{x_\alpha} H, 0], \text{ then } \quad x_\alpha^- = x_\alpha - H, \qquad \text{where } x_\alpha = x \text{ or } y \tag{17}$$

and figure 5 schematically represents the duplication of two particles for two different extensions of the domain: the first 5(a) for an extension with $k_x = 1/2$ and the second 5(b) with $k_x = 1$ ($k_y = 0$ for both of them). With this modification of the boundary conditions, we

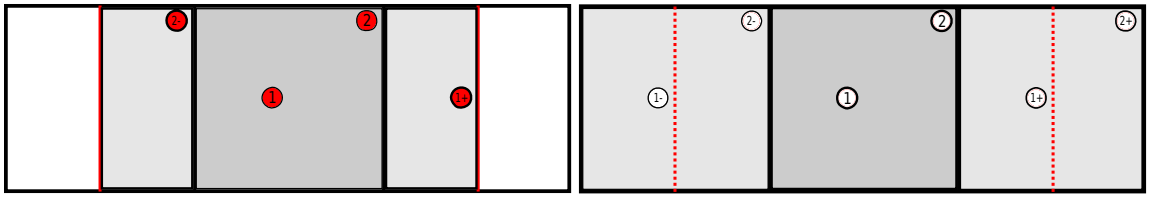

(a) CL $(1/2,0)$ (b) CL $(1,0)$

Figure 5: Schematic description of particles' duplication

decrease the influence of the vertical walls on the computation of the velocity. We can precise that only particles inside the original domain are moved. The new particles are introduced just for improving the computation of the velocity field and their positions are determined only through geometric considerations. In order to limit the influence of the horizontal walls, we also carry out biperiodic boundary conditions such as presented in figure 4(c). The methodology is described more precisely in the next section.

3.3 Sliding biperiodic boundary conditions

Here we describe the changes induced by the Lee-Edwards' biperiodic boundary conditions [4, 8]. The new configuration is presented in figure 6 where we introduced the following nota-

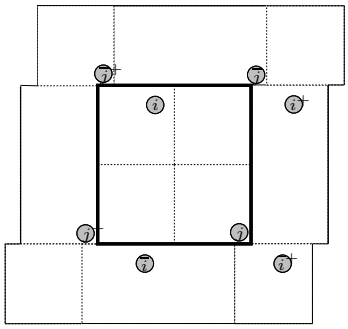

Figure 6: Two particles in a shear flow with biperiodic boundary conditions

tions : i and j design two physical particles, $i^{\pm}$ and $j^{\pm}$ are the $x-$periodic images, as described in last section, $\overline{i}$ and $\overline{j}$ design the images by the biperiodic boundary conditions, and at last $\overline{i}^{\pm}$ and $\overline{j}^{\pm}$ are the $x-$periodic images of particles $\overline{i}$ and $\overline{j}$. In order to keep the shear condition on the upper and lower boundaries of the domain of interest, it is necessary to consider *sliding* boundary conditions as depicted in figure 6. The displacement velocity of the sliding boundary conditions is computed from the definition of the shear rate $\dot{\gamma} = \frac{2U}{H}$; the upper and lower additional domains have hence to move with the velocity:

$$\mathbf{U} = \pm \frac{\dot{\gamma} H}{2} \cdot \mathbf{e}_x \tag{18}$$

so that the positions of the duplicated particles are given by:

$$\overline{\mathbf{x}}_{\alpha}^{n+1} = \overline{\mathbf{x}}_{\alpha}^{n} \pm \frac{\dot{\gamma}}{2} H \Delta t \cdot \mathbf{e}_x \qquad \alpha = i, j \tag{19}$$

3.4 Computation of the distances between particles

Let us now consider the positions and the velocities of the two particles known at times t^n and t^{n-1}. Using the Adams-Bashforth scheme, we are able to compute the positions of physical particles at time t^{n+1} as follows:

$$\mathbf{x}_{\alpha}^{n+1} = \mathbf{x}_{\alpha}^{n} + \frac{\Delta t}{2} \left(3\mathbf{u}_{\alpha}^{n} - \mathbf{u}_{\alpha}^{n-1}\right) \qquad \alpha = i, j \tag{20}$$

and the positions of the corresponding images are computed with the velocity of physical particles:

$$\mathbf{x}_{\alpha}^{\pm n+1} = \mathbf{x}_{\alpha}^{\pm n} + \frac{\Delta t}{2} \left(3\mathbf{u}_{\alpha}^{n} - \mathbf{u}_{\alpha}^{n-1}\right) \quad \text{for the images in } x - \text{direction,} \qquad \alpha = i, j \tag{21}$$

$$\overline{\mathbf{x}}_{\alpha}^{n+1} = \overline{\mathbf{x}}_{\alpha}^{n} + \frac{\Delta t}{2} \left(3\mathbf{u}_{\alpha}^{n} - \mathbf{u}_{\alpha}^{n-1}\right) \quad \text{for the biperiodic images} \qquad \alpha = i, j \tag{22}$$

In the gluey contact model, the condition that must be fulfilled in order to avoid the overlapping is the following:

$$d = \min(d_{ij}, d_{i\overline{j}}, d_{ij^{\pm}}) \geq 0 \tag{23}$$

So we have to compute the distances between the particles. Using (19), (21) and (22), we obtain the following relationships:

$$d_{ij} = \|\mathbf{x}_i\mathbf{x}_j\|^n + \frac{\Delta t}{2}\left((3\mathbf{u}_j^n - \mathbf{u}_j^{n-1}) - (3\mathbf{u}_i^n - \mathbf{u}_i^{n-1})\right)\cdot\mathbf{e}_{ij} \tag{24}$$

$$d_{i\overline{j}} = \|\mathbf{x}_i\overline{\mathbf{x}}_j\|^n + \frac{\Delta t}{2}\left((3\mathbf{u}_j^n - \mathbf{u}_j^{n-1}) - (3\mathbf{u}_i^n - \mathbf{u}_i^{n-1}) \pm \dot{\gamma}\, H\cdot\mathbf{e}_x\right)\cdot\mathbf{e}_{ij} \tag{25}$$

$$d_{ij^{\pm}} = \|\mathbf{x}_i{\mathbf{x}_j}^{\pm}\|^n + \frac{\Delta t}{2}\left((3\mathbf{u}_j^n - \mathbf{u}_j^{n-1}) - (3\mathbf{u}_i^n - \mathbf{u}_i^{n-1})\right)\cdot\mathbf{e}_{ij} \tag{26}$$

In the numerical procedure, the distances between physical particles and all images are computed in order to take the minimum value for the contact model.

4 NUMERICAL RHEOLOGY

As explained in the introduction, determining rheological properties of dense suspensions remains important for many applications. For this purpose, we present here the way of calculating the macroscopic variables from our computations. Let first note $\langle \boldsymbol{X}\rangle_\Omega$ the mean value of $\boldsymbol{X}$ at time t over Ω. We have:

$$\langle \boldsymbol{X}\rangle_\Omega = \frac{1}{\Omega}\int_\Omega \boldsymbol{X}(\mathbf{x})\,\mathrm{d}\Omega \tag{27}$$

By taking the mean value of the stress tensor σ using (27), one gets:

$$\langle\boldsymbol{\sigma}\rangle_\Omega = \langle\boldsymbol{\sigma}_f\rangle_\Omega + \langle\boldsymbol{\sigma}_s\rangle_\Omega \quad \text{with} \quad \begin{cases} \langle\boldsymbol{\sigma}_s\rangle_\Omega = 2\eta_s\langle\dot{\boldsymbol{\varepsilon}}(\mathbf{u})\rangle_{\Omega_s} - \langle p\rangle_{\Omega_s}\mathbf{I}_d + \langle\boldsymbol{\lambda}\rangle_{\Omega_s} \\ \langle\boldsymbol{\sigma}_f\rangle_\Omega = 2\eta_f\langle\dot{\boldsymbol{\varepsilon}}(\mathbf{u})\rangle_{\Omega_f} - \langle p\rangle_{\Omega_f}\mathbf{I}_d \end{cases} \tag{28}$$

where $\langle\boldsymbol{\sigma}_s\rangle_\Omega$ and $\langle\boldsymbol{\sigma}_f\rangle_\Omega$ are respectively the solid and fluid stress tensors. Theoretically, the xy–component of the mean stress tensor in the suspension is given by:

$$\langle\boldsymbol{\sigma}_{xy}\rangle_\Omega = 2\eta_{eff}\langle\dot{\boldsymbol{\varepsilon}}(\mathbf{u})_{xy}\rangle_{\Omega_f} \tag{29}$$

which allows us to write the effective viscosity as follows:

$$\eta_{eff} = \frac{\langle\boldsymbol{\sigma}_{xy}\rangle_\Omega}{\langle\dot{\gamma}\rangle_\Omega} \tag{30}$$

5 RESULTS

In previous papers [7, 9] we analysed the reversibility of Stokes equations with two particles and we studied academic configurations such as three 2D particles in a shear flow. In the following, we will focus on more complicated configurations.

5.1 Influence of computational parameters

In order to obtain relevant results for analysing the rheology of dense suspensions, it is necessary to check the importance of some computational parameters. Namely, we present here the influence of both the penalisation and the number of Uzawa iterations for the convergence of the 2D Stokes flow, and the influence of the mesh size. The example that has been used for this purpose is the 2D suspension of concentration $c \approx 0.24$.

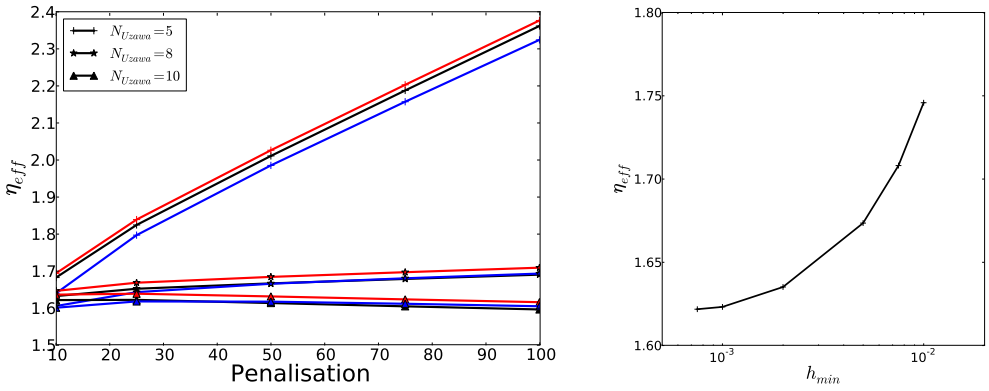

(a) Influence of the penalisation and N_{Uzawa} for the different BC: black $(0,0)$, red $(1/2,0)$ and blue $(1/2,1/2)$

(b) Influence of the mesh size

Figure 7: Influence of the computational parameters on the effective viscosity η_{eff}

The results of the different tests are summed up in figure 7. On figure 7(a) one clearly observes that only 5 Uzawa iterations are not sufficient for obtaining the correct effective viscosity, whereas 8 and 10 Uzawa iterations lead to almost the same viscosity, when taking the penalisation enough small. The same observations can be made for the three different boundary conditions. We also tested the influence of the mesh size on the effective viscosity by fixing all meshing parameters, and then gradually decreasing the value of the minimum authorized size of element, called h_{min}. The lower h_{min} is, the finer the mesh is, which is supposed to enhance the quality of the results. The results of this test are reported on figure 7(b), where we notice that it exists an asymptotic value of the viscosity when refining the mesh. In the following, and for CPU time reasons, we will chose a penalisation of 10, 8 Uzawa iterations and $h_{min} = 10^{-3}$.

5.2 Influence of the contact model

The example presented here is the motion of 13 particles of radius $a = 0.05$ in a 3D shear flow. Initially, the particles are located very close from each other (compacity close to 0.74) in order to have the more contacts possible. Figure 8 shows the evolution of the particles trajectories in the (x, y) plane after $t = 12.5s$. This figure emphasizes the differences induced by choice of the contact model: whereas the particles remain stuck during the whole computation

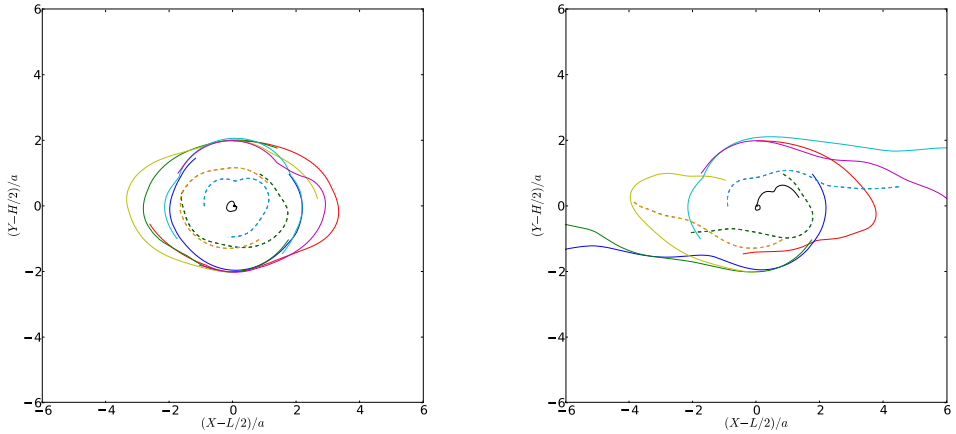

(a) Viscous contact (b) Inelastic collisions

Figure 8: Influence of the contact modelling for the 13-particles case: trajectories of the particles

with the viscous contact model, after a few time steps the cluster of particles disappears with the inelastic collisions model and the particles move away. This is due to the physical nature of the contact models. For the inelastic collisions, the value λ of the Lagrange multiplier can be only positive which means that it acts like a repulsive force between particles. Otherwise, in the viscous model, λ can be either negative or positive, which indicates it acts like a lubrication force: an attractive force is exerced on the particles when they go away from each other.

5.3 Influence of the boundary conditions

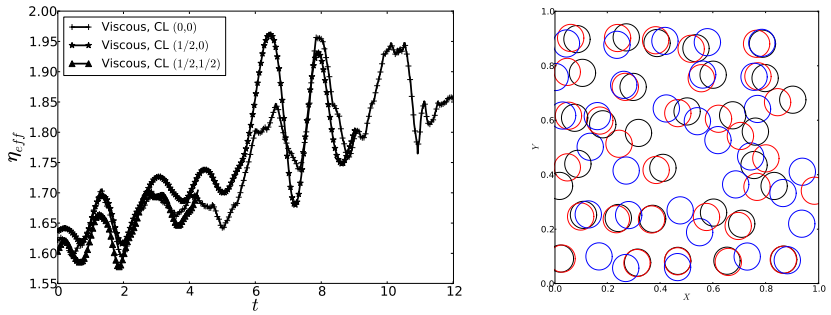

(a) Temporal evolution of η_{eff} (b) Particles position after 4.25s

Figure 9: Influence of the boundary conditions for the 2D suspension of concentration $c \approx 0.24$

In this section we study the rheological behaviour of a 2D suspension of concentration

$c \approx 0.24$ with computations for the three different boundary conditions. Figure 9(a) presents the time evolution of the effective viscosity whereas figure 9(b) shows the position of the particles at $t = 4.25s$. These results point out that boundary conditions can significally affect the trajectories of the particles and hence the rheology of the suspension. Indeed, the biperiodic conditions limit the influence of the upper and lower walls, so that after 4.25s the effective viscosity is lower ($\eta_{eff} \approx 1.64$) than for the two other boundary conditions for which it is almost the same value, $\eta_{eff} \approx 1.66$. At last, the computed values are far from empirical ones ($\sim 2.1 - 2.5$), which emphasizes the importance of 3D effects that are neglected in this study.

6 CONCLUSIONS

Throughout this article, we pointed out the importance of contact modelling as well as the choice of well-suited boundary conditions. The 13-particles example shows a real big difference in the motion of the particles between the two inplemented contact models whereas the 2D suspension example insists on the importance of the boundary conditions. The identification of the rheological parameters indicates that biperiodic boundary conditions limit wall effects that could be an advantage for future computations of dense suspensions. Nevertheless, we repeat here that these are just preliminary results, and in the future 3D computations are mandatory for understanding the behaviour of suspensions.

REFERENCES

[1] R. Glowinski, T.-W. Pan, T.I. Helsa, and D.D. Joseph. A distributed lagrange multiplier/fictious domain method for particulate flows. *Int. J. Multiphase Flows*, 25:755–794, 1999.

[2] B. Maury. A gluey particle model. *ESAIM: Proc.*, 18:133–142, 2007.

[3] A. Lefebvre. Numerical simulation of gluey particles. *M2AN*, 43:53–80, 2009.

[4] A.W. Lees and S.F. Edwards. The computer study of transport process under extreme condition. *J. Phys. C: Solid State Phys.*, 5:1921–1928, 1972.

[5] N.A. Patankar, P. Singh, D.D. Joseph, R. Glowinski, and T.-W. Pan. A new formulation of the distributed lagrange multiplier/fictitious domain method for particulate flows. *Int. J. of Multiphase flow*, 26:1509–1524, 2000.

[6] P. Laure, G. Beaume, O. Basset, L. Silva, and T. Coupez. Numerical methods for solid particles in particulate flow simulations. *European J. Comp. Mechanics*, 16:365–383, 2007.

[7] N. Verdon, A. Lefebvre-Lepot, L. Lobry, and P. Laure. Contact problems for particles in a shear flow. *European J. Comp. Mechanics*, 19:513–531, 2010.

[8] W.R. Hwang, M.A. Hulsen, and H. E. H. Meijer. Direct simulation of particle suspensions in sliding bi-periodic frames. *J. Comp. Physics*, 194:742–772, 2004.

[9] N. Verdon, G. Beaume, A. Lefebvre-Lepot, L. Lobry, and P. Laure. Immersed finite element method for direct numerical simulation of particle suspension in a shear flow. *J. Comp. Physics*, submitted, 2010.